A NANOFIBROUS SCAFFOLD REPRESENTATIVE OF THE CHANGE IN COLLAGEN FIBRIL DIAMETER DISTRIBUTION OF BOVINE ANTERIOR CRUCIATE LIGAMENT UPON INJURY

Zhuldyz Beisbayeva

Bachelor in Chemical and Material Engineering

Submitted in fulfilment of the requirements for the degree of Master of Science in Chemical and Materials Engineering

School of Engineering and Digital Sciences
Department of Chemical and Materials Engineering
Nazarbayev University

53 Kabanbay Batyr Avenue,
Nur-Sultan, Kazakhstan, 010000

Supervisor:
Cevat Erisken, Ph.D.
Department of Chemical and Materials Engineering

August, 2019

Declaration

I hereby, declare that this manuscript, entitled “A Nanofibrous Scaffold Representative of the Change in Collagen Fibril Diameter Distribution of Bovine Anterior Cruciate Ligament Upon Injury” is the result of my own work except for quotations and citations which have been duly acknowledged.

I also declare that, to the best of my knowledge and belief, it has not been previously or concurrently submitted, in whole or in part, for any other degree or diploma at Nazarbayev University or any other national or international institution.

Name: Zhuldyz Beisbayeva
Date: 15.08.2019

Acknowledgements

I wish to thank various people for their valuable contribution to this research work. First of all, I would like to express my appreciation to my supervisor, Dr. Cevat Erisken, for his valuable and constructive suggestions during the planning, development and writing of this research work. I would like to offer my special thanks to my co-supervisor, Dr. Levinus Koole, for his support.

I would also like to thank Nurgul Daniyeva and Rakhima Shamenova, Research Technologists at Nazarbayev University, for their valuable guidance and help with specimen preparation for and imaging with TEM and SEM.

I would like to acknowledge my colleagues Ainur Zhanbassynova, Fariza Mukasheva and Gulzada Kulzhanova from Biomaterials and Regenerative Engineering Laboratory for their admirable collaboration.

Last but not the least, I wish to thank my parents Meirzhan Khanymkhan and Nurzhan Syndash, and my husband Yerkegali, my daughter Nazerke. This work would not have been possible without their love, encouragement, and support of all kinds.

Table of Contents

List of abbreviations

ACL	Anterior Cruciate Ligament
AT	Achilles Tendon
DCM	Dichloromethane
DDSA	Dodecenylsuccinic anhydride
DMF	Dimethylformamide
DPM	Dimethylaminomethyl phenol
ECM	Extracellular matrix
FT	Flexor Tendon
MCL	Medial Collateral Ligament
MNA	Methyl nadic anhydride
PCL	Polycaprolactone
PBS	Phosphate buffer solution
PT	Patellar Tendon
SEM	Scanning Electron Microscopy
TEM	Transmission Electron Microscopy

List of tables and figures

Abstract

More than 200,000 people are suffering from Anterior Cruciate Ligament (ACL) related injuries each year in the US. There is an unmet clinical demand for improving biological attachment between grafts and the host tissue in addition to providing mechanical support. For biological graft integration, it is important to provide physiologically feasible environment for the host cells to enable them to perform their duties. However, behavior of cells during ACL healing and, thus, the mechanism of ACL healing is not fully understood partly due to the absence of appropriate environment to test cell behavior both *in vitro* and *in vivo*. In order to help reveal this mechanism, this study aims at: i) investigating the change in fibril diameter of bovine ACL tissue upon injury, and ii) fabricating nanofiber based scaffolds to represent the morphology and structure of healthy and injured ACL tissues.

It is hypothesized that distribution and mean diameter of ACL collagen fibrils will be altered upon injury and that a nanofiber based scaffold system can be fabricated to mimic such morphological and structural changes. To test this hypothesis, first, an ex vivo ACL injury model was adopted to create an ACL rupture in the bovine knee joint. Then, collagen fibril diameter distribution and mean collagen fibril diameter of both healthy and injured ACL tissues were obtained using Transmission Electron Microscopy (TEM) images. Next, electrospun polycaprolactone (PCL) nanofiber scaffolds were fabricated to prove the concept of changes in collagen fibril diameter distribution and mean diameter. Finally, biomechanical properties of healthy ACL tissues and PCL scaffolds were measured by applying extensional deformation at a rate of 5mm/min.

Findings revealed that the collagen fibril diameter distribution of bovine ACL changed from bimodal to unimodal upon injury with subsequent decrease in mean diameter. PCL scaffold fiber diameter distribution exhibited similar bimodal and unimodal distribution behavior to qualitatively represent the cases of healthy and injured ACL, respectively. In terms of biomechanical properties, the native ACL tissue demonstrated comparable modulus values only with the aligned bimodal PCL scaffolds. There was significant difference between mechanical properties of aligned bimodal and unaligned unimodal PCL scaffolds.

Currently, no data is available for the fabrication and application of nanofibrous scaffolds possessing bimodal distribution for ACL regeneration. Due to absence of such work, it has not been possible to date to fully understand the behavior of ACL cells in injured/healing tissues. The novelty in this study is that it proposes for the first time to investigate the collagen

fiber distribution of bovine ACL tissue under both injured and healthy conditions, and utilization of such knowledge for scaffold design. The fibrous scaffold design, proposed also for the first time, represents a significant departure from the conventional unimodal approach, and is expected to have significant contribution to ACL regeneration efforts.

Chapter 1- Introduction

ACL injuries have an estimated annual incidence of more than 200,000 in the United States only [1]. Anterior Cruciate Ligament (ACL) injuries cannot regenerate but heal slowly resulting with a scar tissue formation due to their poorly vascularized nature and frequency of motion. Unfortunately, currently available clinical procedures are not able to fully repair ACL injuries mainly because of the absence of biological integration between grafts and the host tissue [2]. Adolescents involved in sports requiring jumping/landing and pivoting, such as soccer, handball, football, and basketball are more likely to have ligament tear or rupture as compared to those involved in other activities, with females carrying 3 to 5 times higher risk of injury than their male counterparts [3]. Reports reveal that, more than one third of the people with injured ligament tissue undergo reconstruction surgery each year [1], with an estimated annual cost of more than 4 billion dollars for nonsurgical management of ACL injuries, and about 3 billion dollars for surgical reconstruction of ACL [4].

1.1. Background information about ACL related injuries

There are two mechanisms proposed for ACL related injuries: contact and noncontact [4]. The latter occur in approximately 72% of the cases without a physical contact between individuals and is associated with landing motion, sudden deceleration, or changing direction. Yu and Garrett performed an extensive literature review to suggest that sagittal plane biomechanics are the major mechanism of ACL loading [5]. They reported that increased ACL loading is inevitable when decreased knee flexion angle and increased quadriceps muscle force together with posterior ground reaction force result with an increased knee extension moment. The contact injuries, on the other hand, happen due to valgus collapse of the knee caused by contact with another person [6], and can lead to significant chondral injuries and collateral ligament damage [7]. Whether ACL injuries are associated with autoimmune diseases is still a question requiring intensive research. In one case study, it was found that a patient who had received systemic steroids for a long time can recover after an ACL reconstruction surgery [8]. Obviously, increased ACL loading stretches the collagen bundels/fibers, a major constituent of the tissue, until partial or complete ligament rupture occurs as a result of full disruption of individual collagen fibrils. The micro-/nano-structure of the ligament tissue, therefore, plays a critical role in understanding ACL injuries.

1.2. Structure and composition of ACL

Structurally, ACL is a poorly vascularized connective tissue composing mainly of elastin, glycoproteins, glycosaminoglycans and aligned collagen fibers (mostly type I) surrounded by fibroblast cells. It connects femur and tibia with a basic function of stabilizing the knee joint through resisting anterior tibial translation and rotational loads.

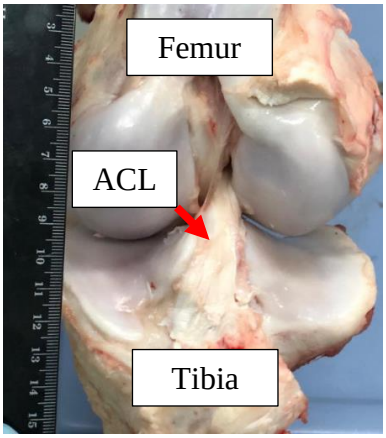

Figure 1.1: Anatomical structure of bovine ACL

Duthon et al. reported on the anatomical structure and properties of the ACL in a review study [9]. Their report defines the cross-section of the human ACL as an irregular geometry, having an area of approximately 34 mm^2 at the femur and 42 mm^2 at the tibia junctions. ACL is composed of small entities called fascicles, which contain fibrils and fibroblasts. Fibrils with diameters of up to 500 nm are formed from subfibrils, and consequently form micro fibrils.

Fibroblasts are ligament cells which produce components of the tissue extracellular matrix (ECM) and form about 20% of total tissue volume. The remaining proportion is the ECM, which in turn contains water by 60-80%. Collagens, mainly types I and III, form 70-80% of the dry volume of the ligament [10]. A summary of ACL tissue composition is provided in Table 1.2.1.

Table 1.2.1: Typical composition of ACL tissue [9]

<table>
<tr><th>Cellular materials (20%)</th><th colspan="3">Extracellular materials (80%)</th></tr>
<tr><td rowspan="3">Fibroblasts</td><td rowspan="3">Water
(60-80%)</td><td colspan="2">Solids (20-40%)</td></tr>
<tr><td>Collagen 70-80%</td><td rowspan="2">Elastin</td></tr>
<tr><td>Type I – 90%
Type III – 10%</td></tr>
</table>

ACL composition and structure are distorted upon injury, and its function is thus compromised as indicated by inferior mechanical properties. The arrangement of collagen fibers in ACL tissue plays a key role in load distribution since wavy parallel arrangement of fibrils provides mechanical resistance to tension force along the fiber axis. During tensile stretch, small part of exerted load on ACL first flattens the crimp fibers, while application of additional load stretches the flattened fibers [9]. The mechanical properties of ACL are directly related to ultrastructure of collagen fibers, therefore an irregular arrangement of collagen fibers in ACL can lead to decreased mechanical resistance to the load leading to ligament rupture. In this regard, diameter and density of collagens are critical attributes of ACL because they ultimately determine mechanical strength of the tissue [11]. Previously published studies about the dependence of mechanical properties on fibril diameter state that proper functioning of ACL requires multimodal distribution of fibril diameter [10]. In such an arrangement, collagen fibrils with smaller diameters are packed into the voids generated by packing of larger fibrils, thus, increasing the packing density reflected into increased mechanical strength. For example, collagen fibril density of ACL was shown to decrease after injury because of remarkable decrease of collagen fibers with larger mean diameter, which disrupts this hierarchical fibril organization [12].

The stress-strain behavior of ACL obtained under tensile loading shows a tri-phasic pattern consisting of (i) the toe region, (ii) the linear region, and (iii) the yield region [13]. The crimp pattern in the collagen fibrils straightens out at low strains, requiring relatively smaller forces, marking the toe region. Resistance force gradually increases in the linear region with elastic deformation. The start of permanent deformation is marked by the yield region. At this juncture, stress decreases due to the disruption of the collagen fibrils, eventually leading to ligament rupture. The following table (Table 1.2.2) shows the previously reported mechanical properties of ACL tissue for different species.

Table 1.2.2: Mechanical properties of ACL tissue

Specie	Age/Weight	Strain rate (mm/min)	Modulus (N/mm)	Maximum load (N)	Source
Human	22–35 years	20	242 ± 28	2160 ± 57	[14]
Sheep	9 months	5	144.97 ± 35.34	548.78 ± 41.44	[1]
Sheep	4 months	6	136.3 ± 28.5	759.2 ± 114.1	[17]
Porcine	NR	5	43.5 ± 7.1	1055.5± 151.2	[15]
Rat	279g	5	37.5± 11.5	47.8± 9.2	[16]
Sheep	NR	60	44.5±12.5	1531.3±180.3	[18]
Bovine	12 months	500	204.1±89.5(MPa)	3317±819	[19]
Bovine	3-7 years	60	577.3±483.1*	4372±1485	[20]
Bovine	Mature	60	NR	4,541±1,417	[21]

NR: Not reported. * recalculated from the source for unit consistency

1.3. In vitro and in vivo injury models for ACL

In the present study, bovine ACL tissue was used to determine the effect of injury on the mean and distribution of collagen fibril diameter. The choice of animal model in an experimental work is a critical component as it needs to possess similarities with human subjects. Bovine ACL is used in this study because cow knee represents a good match with the human knee in both size and proportion [22, 23]. To evaluate the structural changes in ACL tissue upon injury, an injured bovine ACL model was created by applying tensile loading at 5mm/min until rupture. Previously, the diameter of collagen fibrils was reported to exhibit structural changes upon injury, i.e., demonstrate a shift from bimodal to unimodal distribution with a reduced mean fibril diameter (Table 1.3.1). This change is the opposite of structural changes taking place during collagen fibril development, where characteristic unimodal distribution of pediatric/immature collagen fibrils gradually changes to bimodal distribution as the specie matures [24,25].

Table 1.3.1: Fibril diameter changes of different adult species upon injury

Animal	Peak(s) for healthy tissue (nm)		Range Healthy (nm)	Peak for injured tissue (nm)	Range Injured (nm)	Reference
	Smaller	Larger				
Human ACL	~50	~ 120&150	20-200	NR	NR	[11]
Human ACL	75	NR	20-185	71	20-290	[26]
Human ACL	~ 35		10-125	NR	NR	[12]
Rabbit ACL	~ 20	~ 250	10-320	NR	NR	[27]
Rabbit MCL	~ 40	~ 190	20-270	~ 50	40-70	[28]
Bovine ACL	~ 60	~ 120	40-250	NR	NR	[29]
Mouse PT	~ 45	~ 145	15-215	~ 45	15-125	[30]
Rat PT	~ 50	~ 210	20-380	~ 50&170	20-380	[31]
Mouse AT	~ 50	~ 170	10-320	NR	NR	[32]
Mouse FT	~ 60	~ 270	40-400	NR	NR	[23]

NR: Not Reported, MCL: Medial Collateral Ligament, PT: Patellar Tendon, AT: Achilles Tendon, FT: Flexor Tendon

1.4. Choice of scaffold material

Multiple biomaterials including poly(lactic-co-glycolic acid), poly(lactic acid) and polycaprolactone (PCL) have been earlier tested for their capacity to serve as scaffolding material for ACL tissue engineering [33]. Due to its biodegradability with a total degradation time of more than a year [34,35], ease of electrospinability [34], suitability in terms of mechanical properties [1] as well as being in the list of materials approved by the Food and Drug Administration, USA, to be used as materials of construction for a variety of biomedical devices, PCL was selected as the biomaterial for fabricating scaffolds.

To the best of our knowledge based on intensive literature review (Dated 29 July 2019, keywords: injury of bovine ACL, tensile properties of the cow ACL, collagen fiber diameter distribution of bovine ACL, databases: scholar.google.com, NU library e-resources) no prior study exists on the effect of bovine ACL injury on collagen fibril diameter distribution. In this work, ACL injuries were created using an ex vivo extensional deformation on bovine knee joints, and the collagen fibril diameter distribution and mean diameter were determined for both injured and healthy ACL tissues using TEM images. The PCL scaffolds were fabricated using electrospinning technique and evaluated for both diameter distribution and mean fiber diameter. Biomechanical properties of the healthy ACL tissues were characterized and compared with those of PCL scaffolds. It was hypothesized, based on prior findings for human, rabbit and rat

models (Table 1.3.1) that the mean diameter of collagen fibrils will be altered upon injury and that this structural change can be replicated in a synthetic biomaterial scaffold. It is expected that utilization of bimodal and unimodal scaffolds fabricated in this study in *in vitro* and *in vivo* studies will enable regenerative engineering community to better understand behavior of cells in cases of health and injury leading to significant contribution to the efforts of ACL repair or regeneration.

Chapter 2- Materials and methods

This research study involves two major experimental work: i) harvesting ACL tissues from bovine and fabricating electrospun nanofiber scaffolds, and ii) their characterization in terms of diameter of structural components (collagen and PCL for ACL and PCL scaffold, respectively) using TEM/SEM as well as tensile biomechanical properties. Experimental design and procedures followed in the harvesting and characterization of ACL tissue are given in Figure 2.1 below.

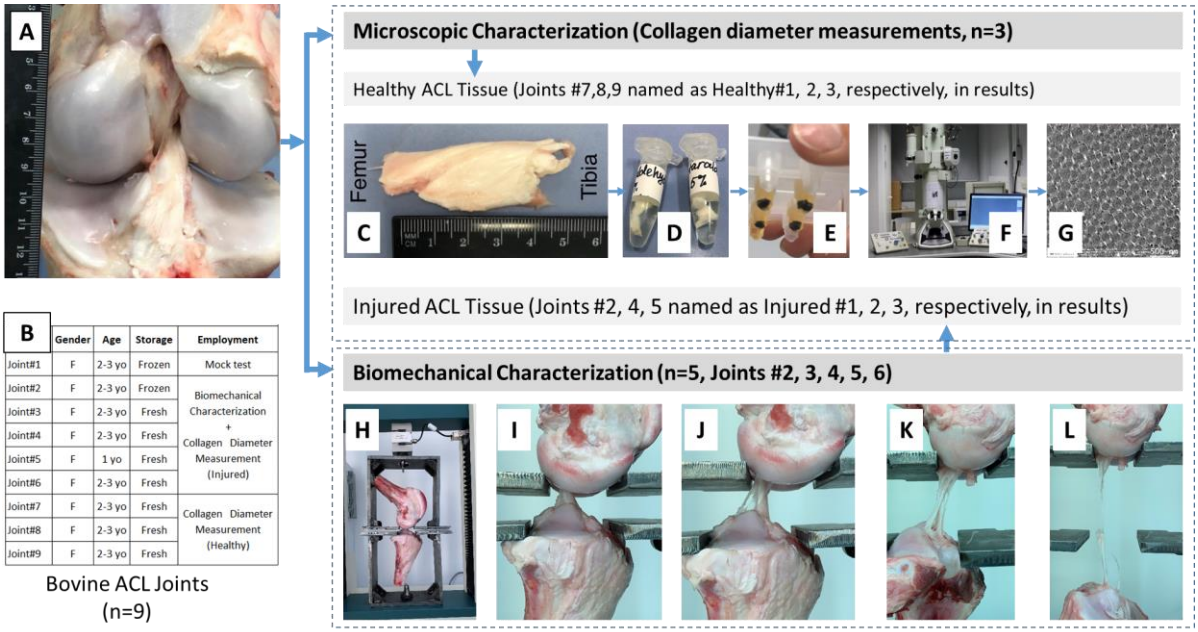

Figure 2.1: Experimental design of and representative images from native ACL harvesting and characterization

2.1. Materials

All the chemicals were procured from Sigma Aldrich with product numbers provided below. Gluteraldehyde (2.5%, Sigma Aldrich, #G5882), osmium tetroxide (1%, Sigma Aldrich, #75633), 0.1 M Phosphate buffer solution (Sigma Aldrich, #P5244), ethanol (Sigma Aldrich, #E7023), propylene oxide (Sigma Aldrich, #82320), epoxy embedding medium 812 substitute (Sigma Aldrich, #45345), epoxy embedding medium hardener DDSA (Sigma Aldrich, #45346), epoxy embedding medium hardener MNA (Sigma Aldrich, #45347), epoxy embedding medium accelerator DMP 30 (Sigma Aldrich, #45348), oil, polycaprolactone

(Sigma-Aldrich, #440744), dichloromethane (Sigma Aldrich, #270997), N-N-Dimethylformamide (Sigma Aldrich #319937).

2.2. Tissue Harvesting

The bovine knee joints were obtained from a local abattoir right after the animal was sacrificed (n=9) and tested for biomechanical properties within 3 hours (n=4) or after storing at -20℃ (n=1). The frozen tissue was thawed at room temperature before the experiment was initiated. All tendons and ligaments of the joint other than ACL were cleared off (Figure 2.1A) to prepare the ACL tissue for biomechanical characterization. More information on the tissue specimens are given in Figure 2.1B.

2.3. Transmission Electron Microscopy Characterization

Collagen fibril diameter and diameter distribution were obtained from Transmission Electron Microscopy (TEM) images of sectioned tissues. For TEM characterization of healthy ACL tissues (n=3/group), location of ACL was identified, extended for better vision, and it was dissected from the bones (Figure 2.1C) to finally obtain a specimen with dimensions of 1mm ×1mm from the midsection of the tissue. Injured ACL tissues were obtained after mechanical rupture of the intact ACL tissues and a specimen with dimensions of 1mm ×1mm from the midsection of the tissue was used for TEM characterization.

The specimens were fixed with 2.5% solution of glutaraldehyde (Figure 2.1D) to prevent any possible alteration of cell structure during processing including cell morphology, volume, and spatial configuration. During fixation, the specimens were initially kept at room temperature and then they were gradually cooled down to 4℃. This type of cooling is necessary to slow down autolytic processes and reduce tissue shrinkage. The specimens were washed with phosphate buffer solution (PBS) three times, each for 10 minutes. To give more stability to the specimen, a secondary fixation was carried out using 1% osmium tetroxide for 2 hours. Osmium tetroxide was used both as a fixative and contrasting material. After fixation, specimens were washed with PBS two times, each for 10 minutes. The specimens were, then, dehydrated through a graded series of 50% ethanol for 40 minutes, 70% ethanol for 12 hours, 96% ethanol for 20 minutes two times, 100% ethanol for 15 minutes two times, a mixture of 100% ethanol and propylene oxide for 10 minutes, and propylene oxide for 15 minutes two times, which was used as a transitional solvent. The graded series of ethanol was used to provide smooth

transitioning to avoid any alterations in tissue structure. Then, the dehydrated specimens were infiltrated using different mixtures of resin and propylene oxide. Resin was prepared from epoxy mix medium components, 812, DDSA (Dodecenylsuccinic anhydride), MNA (Methyl nadic anhydride), in different proportions. Infiltration was conducted to fill blocks of samples with resin in order to make samples hard enough to resist the pressure during sectioning and cutting. Samples were put into 1:1 mixture of resin and propylene oxide for 2 hours at 37℃. Then, mixture was changed to 3:1 proportion for 2 hours at 37℃, followed by pure resin for 12 hours. Next step was embedding with different mixtures of resin and propylene oxide in molds for 24 hours. Polymerization of embedded samples occurred during next two days at 60℃ (Figure 2.1E).

Finally, thin sections were cut perpendicular to the ligament's longitudinal axis using ultra microtome (Boeckeler PT-PC PowerTome Ultramicrotome, USA). This special tool is used for cutting sections of the specimens by movement of the block to the sides by controlled increments over a diamond knife. This device has a trough which is filled with distilled water, where the sections cut are collected. The size of each section was selected to be approximately 60 nm to get images with the best resolution.

In order to take images of ACL sections with high magnification, a Transmission Electron Microscope (JEOL JEM-1400 Plus 120kV TEM) was used (Figure 2.1F). The blocks were adjusted to optimize perpendicular cut of fibrils to obtain cross-sectional views (Figure 2.1G), representing specimens from different locations of the harvested tissue. Approximately 10 sections were imaged for each specimen. In this way approximately 30 sections were obtained for each group of healthy and injured ACL tissues.

2.4. Fibril diameter measurements

A total of ten parallel lines with equal distances were drawn on the TEM images and the diameter of fibrils intersecting these lines were measured. This technique was previously used to measure the fiber diameter of scaffolds imaged using scanning electron microscopy [34]. An image processing software ImageJ (National Institutes of Health, USA) was used to measure diameter of each fibril. A minimum of 100 fibrils was measured for each section and 3 sections were used for each joint. More than 300 representative readings were obtained for each group of healthy and injured ACL tissues. Finally, diameter distribution, mean diameter, and range

were obtained for each group (healthy and injured ACL). A similar approach was employed to measure the fiber diameter of PCL scaffolds using SEM images.

2.5. Nanofiber scaffold fabrication with electrospinning

The scaffolds were fabricated using electrospinning process. PCL solution with two different concentrations (20% w/v, and 40% w/v) were prepared for electrospinning. Briefly, 2g of PCL was dissolved in a 10mL mixture of DCM and DMF (4mL DCM and 6mL DMF) to prepare a solution of 20% PCL. PCL solution with the concentration 40% w/v was prepared by dissolving 4g of PCL in a 10mL mixture of DCM and DMF at 1:1 ratio. The mixtures prepared were stirred gently for 12-16 hours using a magnetic stirrer to ensure homogeneity.

Aligned scaffolds with bimodal fiber distributions were fabricated by co-electrospinning of PCL with 20% and 40% concentrations on a rotating drum. The solutions were transferred to separate syringes facing the drum collector. Solution with 20% PCL was fed at a rate of 0.1mL/h, while solution with 40% PCL was pumped at 0.25mL/h rate. Electrospinning was achieved at 10kV on a drum rotating at 2000 rpm located at 12cm distance. The unaligned fibers were generated by electrospinning the 20% PCL solution at a flow-rate of 0.25mL/h at 10kV and a distance of 12cm onto a stationary collector.

2.6. Mechanical characterization under tension and creation of injured ACL tissues

Biomechanical properties of ACL tissues were measured using a uniaxial material testing machine (Tinius Olsen H25 S, Horsham, PA, USA) equipped with a 5 kN load cell. Tibia-ACL-Femur joint was attached to the unit using a custom-made jaw assembly (Figure 2.1H) and positioned such that axis of the ACL was co-linear with the load axis of the testing device. The specimens were stretched at a constant cross-head speed of 5 mm/min until failure (Figure 2.1I-L). A total of five joints were used to test biomechanical properties. The tensile tests enabled us to create injured ACL tissues and three out of five specimens were employed in fibril diameter measurements representing injured ACL tissue.

Mechanical properties of PCL scaffolds were measured using a uniaxial material testing machine (MTS Criterion Model 43, MTS Systems Co., Eden Prairie, MN, USA) equipped with a 1 kN load cell. Scaffolds were fixed using custom-made jaws and positioned such that the scaffolds are strained in the direction of fiber alignment. The specimens were stretched at a constant cross-head speed of 5 mm/min until failure. A total of three specimens were used to

test mechanical properties of each scaffold group.

2.7. Scanning Electron Microscopy characterization

The scaffolds were first coated with gold with a thickness of 5nm at a current of 20mA using a Turbo-pumped sputter coater (Quotrum Q150T ES, UK). They were, then, imaged using SEM (Crossbeam 540, Zeiss Gemini 2, Germany) with magnifications from 3.5K to 9K.

2.8. Statistical analysis

Comparison of fibril diameter of healthy and injured ACL tissues, diameter of fibers of PCL scaffolds representative of healthy and injured ACL tissues as well as comparison between tensile properties of aligned and unaligned scaffolds were all analyzed using unpaired student-t test. Mechanical properties of scaffolds and native ACL tissue were compared using one way analysis of variance (ANOVA). The difference was considered significant for $p<0.05$.

Chapter 3- Results

3.1. Collagen fibril diameter of ACL

The tissue specimens were processed to yield representative cross-sections of healthy and injured ACL, which were then imaged using TEM. A histogram of fibril diameter distribution for healthy ACL tissue is given in Figure 3.1.1A for each specimen as shown in A1, A2 and A3. Similarly, fibril diameter distribution for injured ACL tissue is given in Figure 3.1.1B for each specimen as shown in B1, B2 and B3. As depicted in Figure 3.1.1, fibril diameter distribution for each specimen follows a similar pattern, i.e., bimodal for healthy and unimodal for injured ACL tissue. The TEM images of healthy ACL tissue (Figure 3.1.1 A1-A3) clearly show that collagen fibrils are well organized and aligned longitudinally along the axis of ligament tissue, extending from femur to tibia, indicated by uniform circular cross-sections. On the contrary, the injured ACL tissue exhibits a disorganized structure where collagen fibrils are unaligned or aligned randomly along the axis of the tissue.

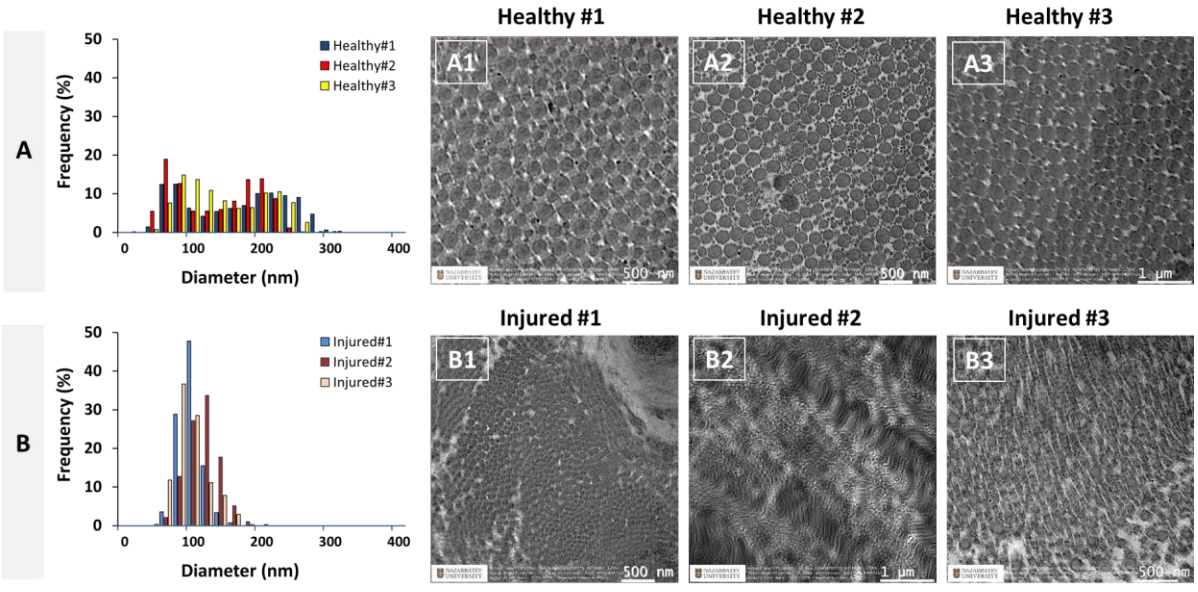

Figure 3.1.1: Diameter distribution of collagen fibrils from (A) healthy and (B) injured ACL tissue and respective (A1-3 and B1-3) TEM images. A1, A2, and A3 correspond to specimens obtained from ACL tissue of each healthy subject (n=3). B1, B2, and B3 correspond to specimens obtained from ACL tissue of each injured subject (n=3).

Combined distribution of collagen fibrils for healthy and injured ACL tissue is given in Figure 3.1.2. For a better qualitative observation of bimodal and unimodal distribution of fibrils, the mean frequency was plotted in the form of histogram (Figure 3.1.2 A) and line graph (Figure 3.1.2B), with respective deviations from the mean indicated by error bars representing standard deviation (SD). Obviously, healthy ACL tissue demonstrated a distribution with two peaks at 73.3±11.5nm and 213±11.5nm while the injured tissue had only one peak at 100±20nm. The range of collagen fibril diameter narrowed from 20-320nm to 40-200nm, with mean fibril diameter decreasing from 137.4±15.9nm to 92.7±10.3nm ($p<0.05$, Figure 3.1.2C). The frequency weighted fibril diameter also decreased from 147.6nm to 102.5nm following a similar trend. Overall, the collagen fibril diameter distribution of bovine ACL changed from a bimodal to unimodal upon injury with narrower range and decreased mean fibril diameter.

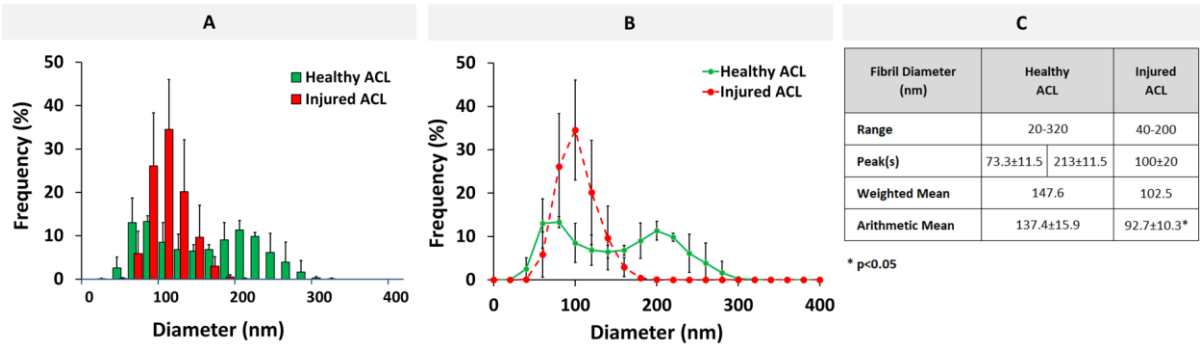

Fibril Diameter (nm)	Healthy ACL		Injured ACL
Range	20-320		40-200
Peak(s)	73.3±11.5	213±11.5	100±20
Weighted Mean	147.6		102.5
Arithmetic Mean	137.4±15.9		92.7±10.3*

* $p<0.05$

Figure 3.1.2. Combined healthy and injured collagen fibril diameter distributions in the form of (A) histogram and (B) line graph, together with (C) descriptive statistics. * indicates statistically significant difference at $p<0.05$ (n=3) and error bars represent SD.

3.2. Fiber diameter of PCL scaffolds

The scaffolds were processed to yield representative cross-sections of aligned and unaligned PCL scaffolds, which were then imaged using SEM. A histogram of fiber diameter distribution for aligned scaffolds is given in Figure 3.2.1A including each specimen as shown in A1, A2 and A3. Similarly, fiber diameter distribution for unaligned scaffolds is given in Figure 3.2.1B for each specimen as shown in B1, B2 and B3. As depicted in Figure 3.2.1, fibril diameter distribution for each specimen follows a similar pattern, i.e., bimodal for aligned and unimodal for unaligned scaffolds representative of healthy and injured tissue, respectively. The SEM images of aligned PCL scaffolds visually show that PCL fibers are organized and aligned longitudinally along the axis of the scaffold. On the contrary, the unaligned PCL scaffold exhibits a disorganized structure where fibers are unaligned or aligned randomly.

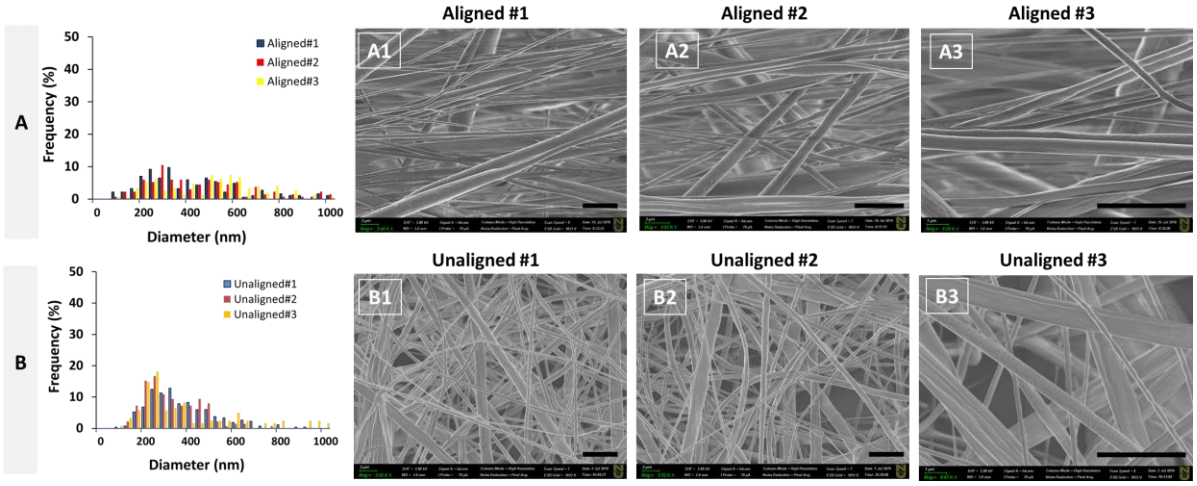

Figure 3.2.1. Diameter distribution of (A) aligned and (B) unaligned PCL fibers and respective (A1-3 and B1-3) SEM images. A1, A2, and A3 correspond to individual specimens obtained from aligned PCL scaffolds (n=3). B1, B2, and B3 correspond to individual specimens obtained from unaligned PCL scaffolds (n=3). Scale bar = 4 μm.

Combined distribution of collagen fibrils for aligned and unaligned PCL scaffolds are given in Figure 3.2.2. For a better qualitative observation of bimodal and unimodal distribution of fibers, the mean frequency was also plotted in the form of histogram (Figure 3.2.2A) and line graph (Figure 3.2.2B), with respective deviations from the mean indicated by error bars representing standard deviation (SD). Obviously, aligned PCL scaffolds demonstrated a distribution with two peaks at 280±40nm and 507±46nm while the unaligned scaffolds had only one peak at 267±46nm. The range of PCL fiber diameter remained the same at 80-1000nm (minor peaks were interruptedly observed at diameters up to 1500nm but ignored due to their little contribution), with mean fiber diameter decreasing from 659±32nm to 370±61nm ($p<0.05$, Figure 3.2.2C). The frequency weighted fiber diameter decreased from 617nm to 388nm. Overall, the aligned and unaligned PCL scaffold fiber diameter distribution were found qualitatively similar to the healthy and injured bovine ACL tissue, respectively.

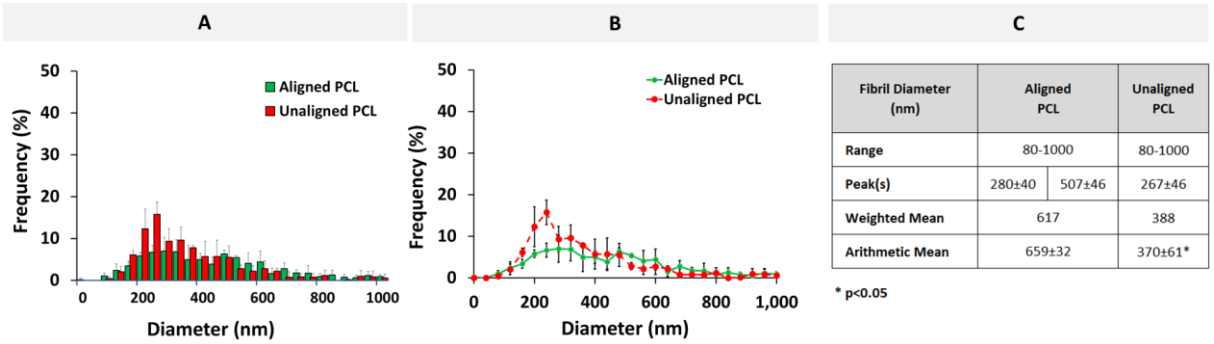

Fibril Diameter (nm)	Aligned PCL		Unaligned PCL
Range	80-1000		80-1000
Peak(s)	280±40	507±46	267±46
Weighted Mean	617		388
Arithmetic Mean	659±32		370±61*

* p<0.05

Figure 3.2.2. Combined aligned and unaligned PCL fiber diameter distributions in the form of (A) histogram and (B) line graph, together with (C) descriptive statistics. * indicates statistically significant difference at p<0.05 (n=3) and error bars represent SD.

3.3. Biomechanical properties of ACL tissue and PCL scaffolds

Biomechanical properties of healthy ACL tissue were evaluated by exposing the specimens to extensional deformation at a rate of 5mm/min until failure. Stress-Strain and Load-Elongation curves of the healthy ACL tissue are shown in Figure 3.3.1A. The tissue follows a typical tri-phase pattern with an initial toe region, followed by linear region, and finally the yield region. Values for the typical parameters of mechanical behavior are given in Figure 3.3.1C. Apparently, the healthy ACL tissue had an ultimate stress and an ultimate strain of 31.9±16.8MPa and 45.8±1.2%, respectively. The tissue exhibits a modulus of 0.8±0.3MPa as determined by the linear region of stress-strain curve. Area under the curve defining the energy accumulated by straining the material, i.e., strain energy density, was calculated as 1140.1±288.5MPa. The tissue was deformed up to a load of 2158.4±733N when strained to an elongation of 21mm (Figure 3.3.1A).

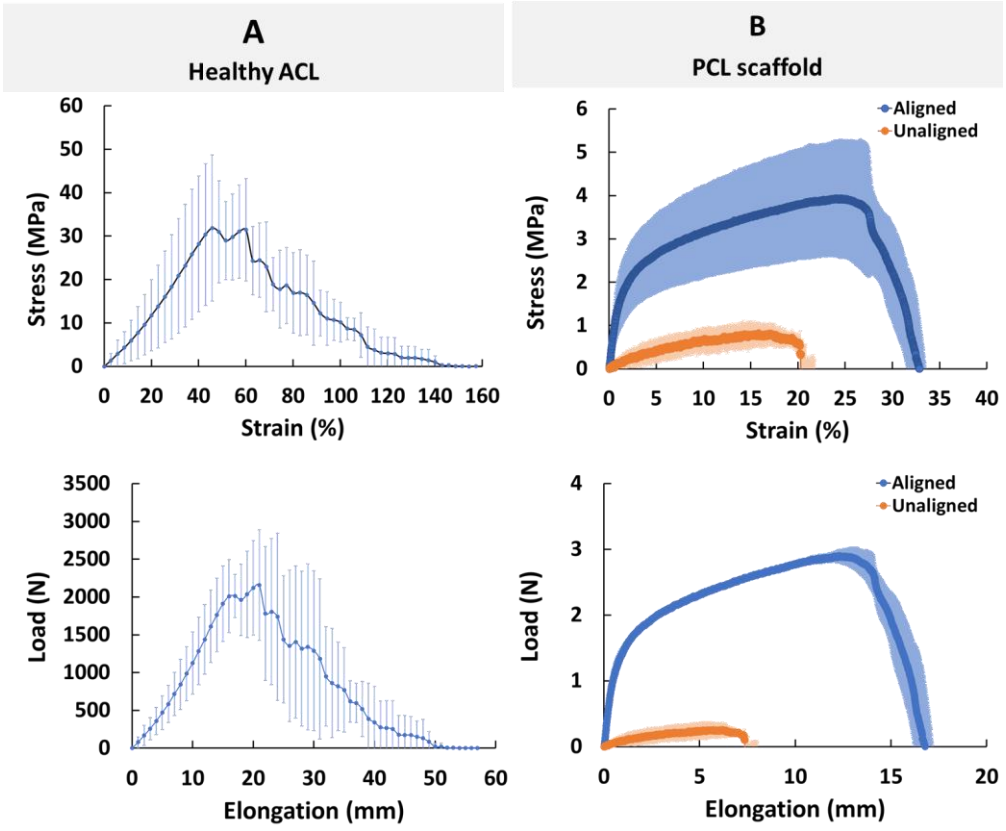

C

	Ultimate Stress (MPa)	Ultimate Strain (%)	Strain at Break (%)	Modulus (MPa)	Strain Energy Density (MPa)	Ultimate Load (N)	Ultimate Strain (mm)
PCL Aligned	3.98±1.36	31.38±2.03	40.80±1.29	1.37±0.52	123.6±43.3	2.93±0.09	12.92±0.84
PCL Unaligned	0.88±0.26 *	17.35±3.15 *	20.47±1.30 *	0.15±0.10 *	11.31±3.86 *	0.28±0.11 *	7.42±0.13 *

* indicates difference between groups at p<0.05.

Figure 3.3.1. Mechanical properties of native ACL tissue and PCL scaffolds. (A) Healthy ACL tissue, (B) aligned and unaligned PCL scaffold with bimodal and unimodal fiber diameter distributions, respectively, and (C) descriptive statistics of PCL scaffolds. * indicates significant difference at p<0.05. Error bars represent SD.

Mechanical properties of PCL scaffold were also evaluated under the same conditions. Stress-Strain and Load-Elongation curves of the PCL scaffolds are shown in Figure 3.3.1B. The PCL scaffolds exhibited a typical tri-phase pattern with an initial toe region, followed by linear region, and finally the yield region. Values for the typical parameters of mechanical behavior of PCL scaffolds are given in Figure 3.3.1C. It was determined that, the aligned PCL scaffolds representing healthy ACL tissue had ultimate stress and ultimate strain of 3.98 ±1.36 MPa and 31.38±2.03%, respectively. Similarly, the unaligned PCL scaffolds representing injured ACL tissue had ultimate stress and ultimate strain of 0.88 ±0.26MPa and 17.35±3.15%, respectively.

The aligned and unaligned scaffolds had moduli of 1.37±0.52MPa and 0.15±0.10MPa, respectively. The strain energy density was calculated as 123.6±43.3MPa and 11.31±3.86MPa for aligned and unaligned scaffolds, respectively. The aligned and unaligned scaffolds were deformed up to a load of 2.93±0.09N and 0.28±0.11N when strained to an elongation of 12.92±0.84mm and 7.42±0.13mm, respectively.

Comparison of the aligned/unaligned scaffolds and native ACL tissue in terms of mechanical properties (Figure 3.3.2) revealed that aligned PCL scaffolds had modulus values similar to native healthy ACL tissue (1.37±0.52MPa versus 0.8±0.3MPa, respectively), all other parameters having values significantly different from the healthy ACL tissue.

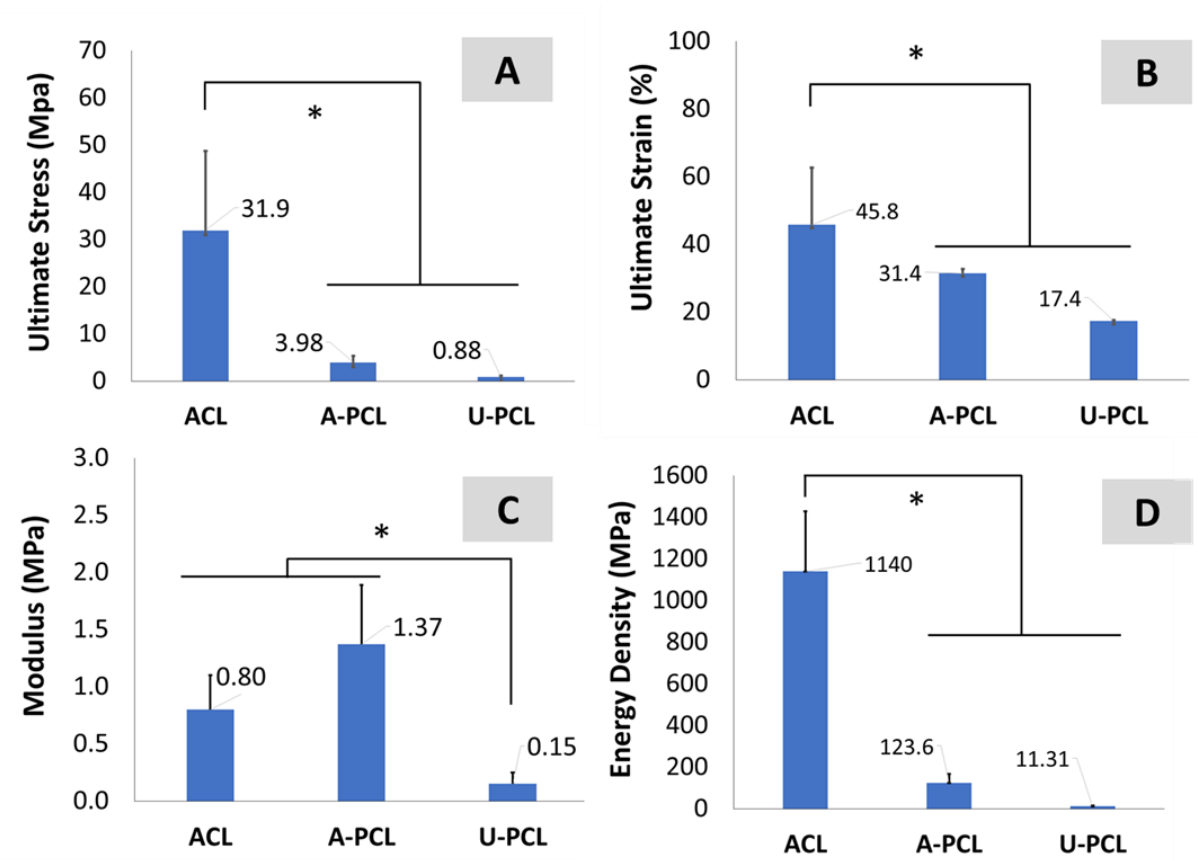

Figure 3.3.2. Comparison of mechanical properties (A: ultimate stress, B: ultimate strain, C: modulus, D: energy density) of PCL scaffolds and native ACL tissue. * indicates significant difference at p<0.05. A-PCL: Aligned PCL, U-PCL: Unaligned PCL.

Chapter 4- Discussion

This study investigated the mean and distribution of diameter of bovine ACL collagen fibrils before and after injury as well as tensile properties of healthy ACL tissue. In addition, fiber diameter distribution and tensile properties of electrospun PCL nanofiber scaffolds were also evaluated to prove the concept of bimodal scaffold design for forthcoming regenerative engineering studies. Briefly, findings revealed that the collagen fibril diameter distribution of bovine ACL changed from bimodal to unimodal upon injury with subsequent decrease in mean diameter. In addition, PCL nanofiber scaffold fiber diameter distribution exhibited similar bimodal and unimodal distribution behavior to qualitatively represent the cases of healthy and injured ACL tissues. The modulus of aligned bimodal PCL nanofiber scaffolds was similar to that of the native ACL tissue.

The function of ACL tissue is directly related to biological and structural characteristics of its constituents. Collagen fibers of ACL, for instance, are regularly arranged bundles of fibrils in a parallel wave pattern along the longitudinal direction which was clearly observed in the TEM images of injured ACL tissues. This organization enhances the mechanical properties of ACL by employing part of exerted load to flatten wavy fibers [11]. Our findings demonstrated that a healthy bovine ACL tissue exhibits an organized/aligned structure of collagen fibrils, while this structure is diminished upon injury. A similar disordered arrangement of collagen fibrils was also reported for completely ruptured human ACLs [26] and rat Patellar Tendon [31]. Obviously, our findings on the organizational changes in the bovine ACL collagen fibrils after injury adds to the existing pool of literature.

One interesting characteristics of tendon/ligament tissues is the reduction in mean collagen fibril diameter and a shift in fibril diameter distribution from bimodal to unimodal distribution. Such a structural variation was previously studied using different species for different tendon/ligament tissues including human ACL [26], rabbit MCL [28] and mouse/rat PT [30,31]. Collagen fibril diameter distribution of rabbit MCL with two peaks at ~40nm and ~190nm changed to exhibit a single peak at ~50nm. The range also changed from 20-270nm to 40-70nm. Similarly, collagen fibril diameter distribution of mouse PT with two peaks at ~45nm and ~145nm changed to exhibit a single peak at ~45nm. The range also changed from 15-215nm to 15-125nm. For tendon/ligament tissues of other species including human ACL, rabbit ACL, bovine ACL, mouse AT and mouse FT, the published studies reported only the mean fibril

diameters and diameter ranges of the healthy tissues without specifically providing the distribution of fibril diameter of the tissue after injury [11,12,23, 27,29,32]. Therefore, this current study also focused on the determination of collagen fibril diameter distribution of bovine ACL before and after injury. Results obtained reveal that the mean fibril diameter reduced significantly upon injury, exhibiting a shift in fibril diameter modality from bimodal to unimodal. A group led by H Lu [29] previously reported on the mean fibril diameter and range as 124.1±22.0nm and 40-250nm, respectively, for the healthy bovine ACL tissue. This is the only relevant study on bovine ACL found in literature, and our results for healthy ACL tissue are comparable with what they reported. More specifically, the mean fibril diameter and the diameter range of the healthy ACL tissue were measured as 137.4±15.9nm and 20-320nm, respectively, in this study.

PCL scaffold fabricated using electrospinning technology qualitatively represent the healthy and injured ACL tissues. Fiber diameter distribution of aligned PCL scaffolds exhibited a bimodal characteristic representing healthy ACL tissue, while that of unaligned PCL scaffolds exhibited a unimodal distribution representing injured ACL tissue. Furthermore, the mean fiber diameter of unaligned PCL scaffolds was significantly smaller than that of aligned scaffolds, representing the decrease in collagen fibril diameter upon injury. Quantitatively, both aligned and unaligned PCL scaffolds possessed larger diameters as compared to collagen fibrils of healthy and injured ACL tissue. Specifically, the mean diameter of aligned PCL scaffolds was calculated as 659±32nm as compared to 137.4±15.9nm mean collagen fibril diameter of healthy ACL tissue. Similarly, the mean diameter of unaligned PCL scaffolds was calculated as 370±61nm as compared to 92.7±10.3nm mean collagen fibril diameter of injured ACL tissue. Although electrospinning is a versatile technique to fabricate nanofibers, there are always limitations associated with this technique one of which is its incapacity to fabricate fibers with diameters as small as native ACL tissue. This is partly related to the choice of scaffold material, which was selected as PCL in this study due to its approved use for biomedical devices. There are published studies reporting smaller PCL fiber diameters obtained using electrospinning, however, they are either reporting diameter of beaded fibers or could not be reproduced [36,37,38].

Collagen fibril diameter and distribution are known as the determinants of tissue mechanical properties and changes in fibril diameter and distribution were found to have a direct effect on the mechanical properties [10, 11, 39]. A bimodal distribution as seen in the

healthy ACL tissue leads to stronger mechanical properties because the interfibril spaces between larger fibrils are filled with smaller fibrils to form a highly packed ECM structure. Upon disruption of this hierarchical structure, the capacity of ligament tissue to resist physiologic loads diminishes, leaving the tissue mechanically weaker. In this study, only the mechanical properties of healthy ACL tissue were tested. Results of tensile tests revealed that the healthy ACL tissue resisted up to a load of 2158.4±733N when strained by 45.8±1.2%. Literature is scarce in terms of tensile properties of bovine ACL and the available studies report data collected at different deformation rates. Unfortunately, to the best of our knowledge, there is no report for the physiologic level deformation rate for ACL tissue. Based on our previous experience [1] and the available literature data, we preferred a deformation rate of 5mm/min. The most relevant study performed with bovine ACL tissue reports a stiffness of 577.3±483.1N/mm and a maximum load of 4372±1485N at 19.3±18% elongation determined at 60mm/min deformation rate [20].

The aligned PCL scaffolds fabricated to represent healthy ACL tissue exhibited similar modulus of elasticity with native ACL tissue (1.37±0.52MPa versus 0.8±0.3MPa, respectively, $p>0.05$). In terms of other parameters tested in this study such as ultimate stress, ultimate strain and energy density, the native ACL tissue was superior to both aligned and unaligned PCL scaffolds. A comparison within the two scaffold groups demonstrated that aligned PCL scaffolds were superior to their unaligned counterparts in terms of all tensile test parameters, which is also in agreement with previously published results of tensile properties of aligned and unaligned PCL scaffolds [40,41].

This study certainly has some methodological limitations that influenced the interpretation of the findings from this research. Firstly, the mechanical properties of injured ACL tissue could not be evaluated due to unavailability of necessary instrumentation. Such an evaluation would allow for a comparison between unaligned PCL scaffolds and injured PCL tissue in terms of mechanical properties. In addition, fiber diameter distribution of the PCL scaffolds was similar to collagen fibril diameter distribution of the native ACL tissue qualitatively. Quantitatively, both mean fiber diameter and diameter distribution of PCL scaffolds were different from ACL tissue due to some obvious factors discussed in the previous paragraphs. Therefore, in this regard, this study can be considered as a proof of concept work and further investigation is needed to fabricate scaffolds with comparable mean diameter and diameter distribution. Furthermore, in the present study, mechanical property of ACL tissue

was tested by applying uniaxial tensile load to the Femur-ACL-Tibia complex, while sagittal plane (anatomical orientation) biomechanics are the major mechanism of ACL loading [42]. This point should be taken into consideration when designing experiments of similar work in the future.

Chapter 5- Conclusion

In the current research, morphological and structural characteristics such as collagen fibril organization, mean diameter and diameter distribution of native bovine ACL tissue were studied before and after injury. Further, nanofiber scaffolds representing structural properties of both healthy and injured ACL tissues were formed using electrospinning. Findings revealed that the collagen fibril diameter distribution of bovine ACL changed from bimodal to unimodal upon injury with subsequent decrease in mean diameter. PCL scaffold fiber diameter distribution exhibited similar bimodal and unimodal distributions to qualitatively represent the cases of healthy and injured ACL tissues, respectively. The native ACL tissue demonstrated comparable modulus values only with the aligned bimodal PCL scaffolds. A comparison of mechanical properties of aligned bimodal and unaligned unimodal PCL scaffolds yielded significant difference between the two groups. Currently, no data is available for the fabrication and application of nanofibrous scaffolds possessing bimodal distribution for ACL regeneration. Such a scaffold design, proposed here for the first time for ACL repair and regeneration, is a deviation from the conventional unimodal approach. Findings of this study are, therefore, expected to have significant impact on the efforts of orthopedic research community to solve an important societal and economic healthcare problem.

Reference list

[1] Gurlek, A. C., Sevinc, B., Bayrak, E., & Erisken, C. (2017). Synthesis and characterization of polycaprolactone for anterior cruciate ligament regeneration. *Materials Science and Engineering: C*, *71*, 820-826.

[2] Lu, H. H., & Thomopoulos, S. (2013). Functional attachment of soft tissues to bone: development, healing, and tissue engineering. *Annual review of biomedical engineering*, *15*, 201-226.

[3] Lohmander, L. S., Englund, P. M., Dahl, L. L., & Roos, E. M. (2007). *The Long-term Consequence of Anterior Cruciate Ligament and Meniscus Injuries. The American Journal of Sports Medicine, 35(10), 1756–1769.*doi:10.1177/0363546507307396

[4] Sepúlveda, F., Sánchez, L., Amy, E., & Micheo, W. (2017). *Anterior Cruciate Ligament Injury: Return to Play, Function and Long-Term Considerations. Current Sports Medicine Reports, 16(3), 172–178.*doi:10.1249/jsr.0000000000000356

[5] Yu, B., & Garrett, W. E. (2007). Mechanisms of non-contact ACL injuries. *British journal of sports medicine*, *41*(suppl 1), i47-i51.

[6] Olsen, O.-E., Myklebust, G., Engebretsen, L., & Bahr, R. (2004). *Injury mechanisms for Anterior Cruciate Ligament Injuries in Team Handball. The American Journal of Sports Medicine, 32(4), 1002-1012.* doi: 10.1177/0363546503261724

[7] Salem, H. S., Shi, W. J., Tucker, B. S., Dodson, C. C., Ciccotti, M. G., Freedman, K. B., & Cohen, S. B. (2018). Contact Versus Noncontact Anterior Cruciate Ligament Injuries: Is Mechanism of Injury Predictive of Concomitant Knee Pathology? *Arthroscopy: The Journal of Arthroscopic & Related Surgery*, *34*(1), 200-204

[8] Ushio, T., Okazaki, K., Mizu-uchi, H., Hamai, S., Akasaki, Y., & Nakashima, Y. (2018). Anterior cruciate ligament reconstruction in a patient who has received systemic steroids for autoimmune disease. *Asia-Pacific journal of sports medicine, arthroscopy, rehabilitation and technology*, *11*, 12-14.

[9] Duthon, J.V., Barea, C., Abrassart, S., Fasel, J.H., Fritschy, D., &Menetrey, J. (2005) Anatomy of the anterior cruciate ligament. Knee Surgery, Sports traumatology, Arthroscopy, 14(3), 204-213. Doi: 10.1007/s00167-005-0679-9

[10] M. Marieswaran, I.Jain, B. Garg, V. Sharma, and D. Kalyanasundaram, A Review on Biomechanics of Anterior Cruciate Ligament and Materials for Reconstruction (2018). Applied Bionics and Biomechanics. DOI: 10.1155/2018/4657824

[11] Zhu, J., Zhang, X., Ma, Y., Zhou, C., & Ao, Y. (2012). Ultrastructural and morphological characteristics of human anterior cruciate ligament and hamstring tendons. *The Anatomical Record: Advances in Integrative Anatomy and Evolutionary Biology*, *295*(9), 1430-1436.

[12] Ochi, M., Murao, T., Sumen, Y., Kobayashi, K., & Adachi, N. (1999). Isolated posterior cruciate ligament insufficiency induces morphological changes of anterior cruciate ligament collagen fibrils. *Arthroscopy: The Journal of Arthroscopic & Related Surgery*,

15(3), 292-296.

[13] Allen, C. R., Livesay, G. A., Wong, E. K., & Woo, S. L. (1999). Injury and reconstruction of the anterior cruciate ligament and knee osteoarthritis. *Osteoarthritis and cartilage*, *7*(1), 110-121.

[14] Woo, S. L. Y., Hollis, J. M., Adams, D. J., Lyon, R. M., & Takai, S. (1991). Tensile properties of the human femur-anterior cruciate ligament-tibia complex: the effects of specimen age and orientation. *The American journal of sports medicine*, *19*(3), 217-225.

[15] Rodríguez, C., García, T. E., Montes, S., Rodríguez, L., & Maestro, A. (2015). In vitro comparison between cortical and cortico-cancellous femoral suspension devices for anterior cruciate ligament reconstruction: implications for mobilization. *Knee Surgery, Sports Traumatology, Arthroscopy*, *23*(8), 2324-2329.

[16] Ohtera, K., Zobitz, M. E., Luo, Z. P., Morrey, B. F., O'Driscoll, S. W., Ramin, K. D., & An, K. N. (2002). Effect of pregnancy on joint contracture in the rat knee. *Journal of Applied Physiology*, *92*(4), 1494-1498.

[17] Meller, R., Willbold, E., Hesse, E., Dreymann, B., Fehr, M., Haasper, C., & Witte, F. (2008). Histologic and biomechanical analysis of anterior cruciate ligament graft to bone healing in skeletally immature sheep. *Arthroscopy: The Journal of Arthroscopic & Related Surgery*, *24*(11), 1221-1231.

[18] Weiler, A., Peine, R., Pashmineh-Azar, A., Abel, C., Südkamp, N. P., & Hoffmann, R. F. (2002). Tendon healing in a bone tunnel. Part I: Biomechanical results after biodegradable interference fit fixation in a model of anterior cruciate ligament reconstruction in sheep. *Arthroscopy: The Journal of Arthroscopic & Related Surgery*, *18*(2), 113-123.

[19] Torre, M., Di Feo, F., De Angelis, G., Ruspantini, I., Frustagli, G., & Chistolini, P. (2003). ACL reconstruction by bone-patellar tendon-bone graft: mechanical evaluation of the elastic modulus and failure modes. *Journal of Orthopaedics and Traumatology*, *4*(2), 69-75.

[20] Diotalevi, L., Petit, Y., Brailovski, V., Nichols, S., Marchionatti, E., & Wagnac, É. (2018). Quasi-static tensile properties of the Cranial Cruciate Ligament (CrCL) in adult cattle: towards the design of a prosthetic CrCL. *Journal of the mechanical behavior of biomedical materials*, *79*, 239-245.

[21] Niehaus, A. J., Anderson, D. E., Johnson, J. K., & Lannutti, J. J. (2013). Comparison of the mechanical characteristics of polymerized caprolactam and monofilament nylon loops constructed in parallel strands or as braided ropes versus cranial cruciate ligaments of cattle. *American journal of veterinary research*, *74*(3), 381-385.

[22] Xerogeanes, J. W., Fox, R.L., Takeda, Y., Ki,, H.-S., Ishibashi, Y., Carlin, G.J.,& Woo, S.L.-Y. (1998). A Functional comparison of Animal anterior cruciate ligament models to the human anterior cruciate ligament. Annals Of Biomedical Engineering, 26(3), 345-352. Doi: 10.1114/1.91

[23] Proffen, B. L., McElfresh, M., Fleming, B. C., & Murray, M. M. (2012). A comparative anatomical study of the human knee and six animal species. *The Knee*, *19*(4), 493-499.

[24] Ezura, Y., Chakravarti, S., Oldberg, Å., Chervoneva, I., & Birk, D. E. (2000). Differential expression of lumican and fibromodulin regulate collagen fibrillogenesis in developing mouse tendons. *The Journal of cell biology*, *151*(4), 779-788.

[25] Schmidt, E. C., Chin, M., Aoyama, J. T., Ganley, T. J., Shea, K. G., & Hast, M. W. (2019). Mechanical and microstructural properties of pediatric anterior cruciate ligaments and autograft tendons used for reconstruction. *Orthopaedic journal of sports medicine*, *7*(1), 2325967118821667.

[26] Neurath, M. F., & Stofft, E. (1992). Collagen ultrastructure in ruptured cruciate ligaments: an electron microscopic investigation. *Acta orthopaedica Scandinavica*, *63*(5), 507-510.

[27] Hart, R. A., Akeson, W. H., Spratt, K., & Amiel, D. (1999). Collagen fibril diameter distributions in rabbit anterior cruciate and medial collateral ligaments: changes with maturation. *The Iowa orthopaedic journal*, *19*, 66.

[28] Woo, S. L., Takakura, Y., Liang, R., Jia, F., & Moon, D. K. (2006). Treatment with bioscaffold enhances the the fibril morphology and the collagen composition of healing medial collateral ligament in rabbits. *Tissue engineering*, *12*(1), 159-166.

[29] Qu, D., Chuang, P. J., Prateepchinda, S., Balasubramanian, P. S., Yao, X., Doty, S. B., & Lu, H. H. (2016). Micro-and ultrastructural characterization of age-related changes at the anterior cruciate ligament-to-bone insertion. *ACS Biomaterials Science & Engineering*, *3*(11), 2806-2814.

[30] Johnston, J. M., Connizzo, B. K., Shetye, S. S., Robinson, K. A., Huegel, J., Rodriguez, A. B., & Soslowsky, L. J. (2017). Collagen V haploinsufficiency in a murine model of classic Ehlers–Danlos syndrome is associated with deficient structural and mechanical healing in tendons. *Journal of Orthopaedic Research*, *35*(12), 2707-2715.

[31] Muellner, T., Kwasny, O., Loehnert, V., Mallinger, R., Unfried, G., Schabus, R., & Plenk Jr, H. (2001). Light and electron microscopic study of stress-shielding effects on rat patellar tendon. *Archives of orthopaedic and trauma surgery*, *121*(10), 561-565.

[32] Gehwolf, R., Wagner, A., Lehner, C., Bradshaw, A. D., Scharler, C., Niestrawska, J. A., & Traweger, A. (2016). Pleiotropic roles of the matricellular protein Sparc in tendon maturation and ageing. *Scientific reports*, *6*, 32635.

[33] Alshomer, F., Chaves, C., & Kalaskar, D. M. (2018). Advances in Tendon and Ligament Tissue Engineering: Materials Perspective. *Journal of Materials*, *2018*.

[34] Erisken, C., Kalyon, D. M., & Wang, H. (2008). A hybrid twin screw extrusion/electrospinning method to process nanoparticle-incorporated electrospun nanofibres. *Nanotechnology*, *19*(16), 165302.

[35] Woodruff, M. A., & Hutmacher, D. W. (2010). The return of a forgotten polymer—Polycaprolactone in the 21st century. *Progress in polymer science*, *35*(10), 1217-1256.

[36] Liverani, L., & Boccaccini, A. (2016). Versatile production of poly (epsilon-caprolactone) fibers by electrospinning using benign solvents. *Nanomaterials*, *6*(4), 75.

[37] Kanani, A. G., & Bahrami, S. H. (2011). Effect of changing solvents on poly (ε-caprolactone) nanofibrous webs morphology. *Journal of Nanomaterials*, *2011*, 31.

[38] Ghobeira, R., Asadian, M., Vercruysse, C., Declercq, H., De Geyter, N., & Morent, R. (2018). Wide-ranging diameter scale of random and highly aligned PCL fibers electrospun using controlled working parameters. *Polymer*, *157*, 19-31.

[39] Ottani, V., Raspanti, M., & Ruggeri, A. (2001). Collagen structure and functional implications. *Micron*, *32*(3), 251-260.

[40] Moffat, K. L., Kwei, A. S. P., Spalazzi, J. P., Doty, S. B., Levine, W. N., & Lu, H. H. (2008). Novel nanofiber-based scaffold for rotator cuff repair and augmentation. *Tissue Engineering Part A*, *15*(1), 115-126.

[41] Jahani, H., Kaviani, S., Hassanpour-Ezatti, M., Soleimani, M., Kaviani, Z., & Zonoubi, Z. (2012). The effect of aligned and random electrospun fibrous scaffolds on rat mesenchymal stem cell proliferation. *Cell Journal (Yakhteh)*, *14*(1), 31.

[42] Garrett, W. E. (2007). Mechanisms of non-contact ACL injuries. *British journal of sports medicine*, *41*(suppl 1), i47-i51